Evaluation of the Forward Scattering Spectrometer Probe. Part I: Electronic and Optical Studies

JAMES E. DYE AND DARREL BAUMGARDNER

National Center for Atmospheric Research,[1] Boulder, CO 80307

(Manuscript received 9 January 1984, in final form 11 July 1984)

ABSTRACT

Laboratory studies of the Forward Scattering Spectrometer Probe (FSSP), were conducted to better understand the operation, to determine limitations and to define the measurement accuracy of the instrument for airborne cloud physics research. The studies included electronic checks of the instrument sensitivity to simulated particles of different sizes, airspeeds and arrival rates; measurement of important aspects of the optical configuration; and intercomparisons of six different FSSPs in a small wind tunnel with a droplet spray. The tests demonstrated measurement differences between various probes in several areas as well as areas in which there was reasonable agreement. Part of the differences can be attributed to different feature and design specifications of different probes as changes were made to improve the FSSP. Areas in which care needs to be taken in the calibration and processing of data from the FSSP are identified.

1. Introduction

The Forward Scattering Spectrometer Probe (FSSP)[2] (Knollenberg, 1981) has been used extensively over the last several years for studying cloud droplet as well as other aerosol distributions. Since its development (Knollenberg, 1976) there have been a number of limited studies of the FSSP (Gayet, 1976; Pinnick *et al.*, 1981; Cerni, 1983) and comparisons among them (Breed and Dye, 1982) and with other instruments (Mossop, 1983; Baumgardner, 1983). Studies such as these, as well as extensive use of the FSSP by many research organizations, has focused attention on the need for further study of the accuracy, reliability and limitations of the FSSP. In order to answer some of these questions, a number of detailed optical and electronic studies and intercomparisons were conducted. The results of these studies along with recommendations regarding the use of the FSSP are presented in this paper.

As part of these studies a small workshop was held at the National Center for Atmospheric Research (NCAR) during December 1981. The six FSSPs and one ASSP that were studied at the workshop encompassed the whole range of possible modifications that have been made to the FSSP since its first development. These differences are illustrated in Table 1, and will be discussed in more detail as they appear in the text. The probes shown in Table 1 are operated by the following organizations: number 1—South Dakota School of Mines and Technology; number 2—Atmospheric Environment Service, Canada; number 5—NCAR, Convective Storms Division; number 6—NCAR, Research Aviation Facility; number 12—University of Wyoming; number 66—University of Washington; ASSP—University of Wyoming.

2. Principles of operation

A 632.8 nm laser beam, focused to a diameter of approximately 0.2 mm at the object plane, is projected across the probe's sampling aperture onto an opaque dump spot (Fig. 1). The light that is scattered forward by particles passing through the beam is collected from a solid angle defined by the diameter of the dump spot, the opening in the sample tube and the distance of the particle from the dump spot. This light then passes through a prism and collecting lens and enters a beam splitting prism. One portion of the light from the prism illuminates a photodetector that is referred to as the *signal* detector, while the other portion falls on a photodetector that has been partially masked to detect only that light from the larger scattering angles. This defines an annulus of scattered light and, hence, is referred to as the *annulus*. The output of both detectors are amplified and conditioned, with the output of the annulus typically amplified 2 to 3 times more than the signal. Particles passing through the beam far from the focal plane scatter proportionally more light into the annulus than those close to the focal plane. Thus, the depth-of-field (DOF) can be established by an electronic

[1] The National Center for Atmospheric Research is sponsored by the National Science Foundation.

[2] The FSSP is manufactured by Particle Measurement Systems, Boulder, Colorado.

TABLE 1. Optical and electronic configurations of several FSSPs and the ASSP. SN denotes serial number.

	FSSP SN 1	FSSP SN 2[a]	FSSP SN 5[a]	FSSP SN 6[a]	FSSP SN 12[a]	FSSP SN 66	ASSP
Optical configuration							
Beam diameter (mm)	0.153	0.188	0.204	0.183	0.178	0.192	0.178
Depth-of-field (mm)	2.250	3.100	3.000	2.740	2.650	2.850	2.650
Dump spot diameter (mm)	4.0	4.0	4.0	4.0	6.0	4.0	4.0
Scattering angles (°)	4.0–18.5	3.0–12.7	3.0–12.7	3.0–12.7	4.6–12.8	3.0–12.7	7.0–16.0
Condensing lens focal length (mm)	50	55	55	55	55	55	55
Electrical configuration and response times							
Sets of PHA comparator voltages	1	1	1	4	4	4	1
Delay line installed	No	Yes	No	No	Yes	Yes	No
Slow reset delay time (μs)	5.3	7.7	5.1	5.4	5.6	9.1	4.2
Fast reset delay time (μs)	NA[b]	2.2	NA	2.9	2.1	2.6	NA
Delay between input pulse and transit gate (μs)	2.4	0.6	4.3	2.5	2.7	1.0	—[c]
Min. transit gate width (μs)	1.6	1.3	1.6	0.5	—[c]	1.0	1.4
Pulse width at 3 dB Roll-off of signal voltage (μs)	0.8	0.7	1.5	0.7	0.8	0.6	—[c]
Pulse width at 3 dB Roll-off of annulus voltage (μs)	0.8	2.0	1.7	0.7	0.8	0.8	—[c]
Frequency at 3 dB Roll-off of signal voltage (Khz)	165	135	125	145	165	180	—[c]
Frequency at 3 dB Roll-off of annulus voltage (Khz)	150	135	100	175	165	180	—[c]
Activity correction factor	0.55	0.81	0.71	0.71	0.56	0.49	0.63

[a] These probes have been modified since their original fabrication.
[b] Not applicable.
[c] Not measured.

comparison of the annulus and signal voltages. The voltage output of the signal and annulus detectors are shown as a function of position for a uniform scatterer being moved along the beam in Fig. 2.

The particle size can be predicted from the measured light intensity using Mie scattering theory with the knowledge of the wavelength of the incident light, particle index of refraction and the scattering angles over which the light is collected. Pinnick *et al.* (1981) have corroborated the response of the FSSP with theoretical Mie calculations for three markedly different indices of refraction with uniform particles from 2 to 40 μm in diameter. The voltage of the signal is converted to a particle size using a 15 channel pulse height analyzer (PHA) whose comparator levels are preset corresponding to certain size intervals. Early models use a single set of comparator voltages to set the size intervals and rely only on gain changes to change-size ranges. Later models incorporate a separate set of comparator voltages for each size range matched to the appropriate portion of the Mie scattering curve at each range.

To eliminate particles passing near beam edges, an electronic average of the *transit times* of particles

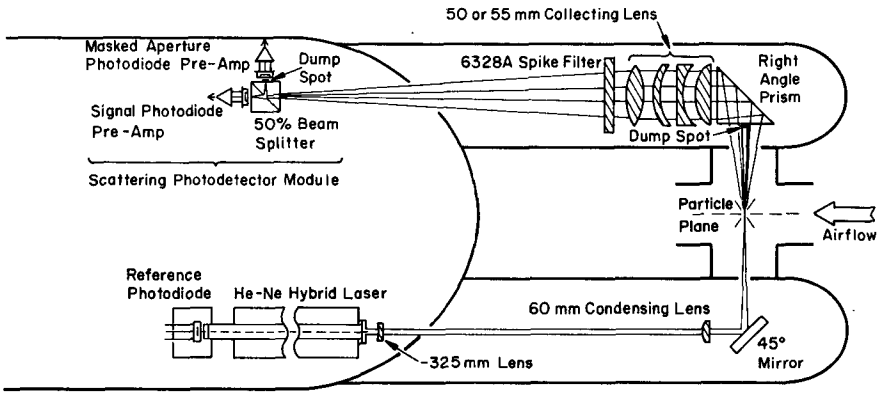

FIG. 1. A schematic showing the optical path and components in the FSSP.

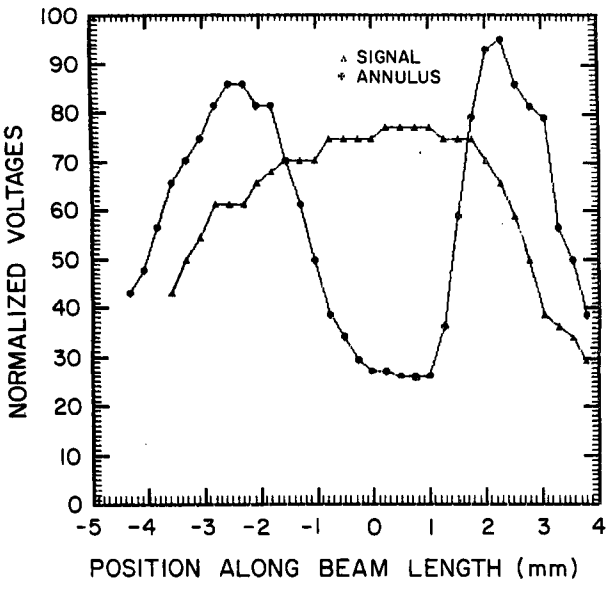

FIG. 2. The output voltages of the signal and annulus photodetectors are shown as a function of position as a thin, translucent scattering medium is moved horizontally in the beam. The positions where the two sets of voltages cross over define the boundaries of the depth-of-field.

passing within the DOF is maintained. Particles whose transit times are shorter than the average are *velocity rejected* while particles with longer than the average transit times are *velocity accepted.* For this latter case, the FSSP generates a *gated strobe* which is sent to the data system with the corresponding size information for that particle.

After a particle exits the beam, there is a reset period, or *delay time,* during which the particle is sized and other housekeeping procedures are completed. For older probes the delay time for all particles is typically 6 to 10 μs, depending upon the probe. For newer probes the delay time is approximately 6 μs for particles passing within the DOF and about 3 μs for those out of the DOF. These two times are referred to as *slow* and *fast delays,* respectively. During these periods the probe is insensitive to transitting particles. In order to correct for this undercounting, modifications have been made to some of the older probes and all of the newer probes so that the *activity* can be measured. The activity output increments a counter in proportion to the sum of the particle transit time and the subsequent delay and reset times. Over a given sampling period this activity count gives a measure of the amount of time the electronics were busy. Some probes use a *total reset* and/or *total strobes* or *fast reset* output instead of the activity. The total reset output produces a count for each particle detected anywhere in the beam. The fast reset output (on newer probes) produces a count for each particle which was not in the DOF. The total strobes output produces a count whenever a particle passes within the DOF and is within the sizing limits of the PHA, regardless of whether or not it is velocity accepted. The total strobe output, along with any one of the other three outputs are essential to the correction methods discussed below. A flow chart of events as a particle transit is detected and processed by the FSSP is shown in Fig. 3a, and a block diagram of the electronics discussed in the following section in Fig. 3b. This flow chart is representative of most new probes, but there are differences in some of the probes.

3. Electronic response tests

Systematic checks were made of the electronic functions considered to be important for proper sizing and counting. In particular, it was of interest to examine the behavior at particle rates in excess of 100 kHz, the maximum rate recommended by the manufacturer. With the typical sensitive sampling rate of the FSSP of about 240 cm^{-3} s^{1} for an aircraft flying at 100 m s^{-1}, the 100 kHz rate will be exceeded when particle concentrations exceed 400 cm^{-3}. It was also important to examine the effects of airspeed on the FSSP's measurement of particle size and concentration.

a. Electronic operating principles

The electronics in the FSSP may be divided into six stages based upon specific functions as shown in Fig. 3b. A simplified timing sequence within the electronics as a particle passes through the beam is illustrated in Fig. 4. The first stage consists of the photodetection circuit. The second stage restores baseline shifts introduced by the AC coupling to the previous stage and provides additional amplification of the signal and annulus voltages. The third stage compares the annulus and signal voltages and provides the decision criteria that defines the DOF. The fourth stage consists of the PHA, which categorizes the signal voltage into one of 15 size classes. Once the peak value is determined by the PHA, it is encoded for subsequent transmission to the data system. If the peak value is greater than the lower limit of the first PHA threshold, this stage of electronics also generates a pulse (the *transit gate*) whose width is proportional to the transit time of the particle through the beam. Some probes determine the transit width as the time between crossings of a preset threshold, while many newer ones use a delay line to measure the width of the signal pulse at half its maximum value. The latter method was implemented to minimize the effect of particle size on the length of the transit pulse.

The fifth stage of the electronics maintains a counter whose value is proportional to a pseudo-average transit period of all particles passing within the DOF that were within the size limits. When a particle transits the beam, the count from another counter

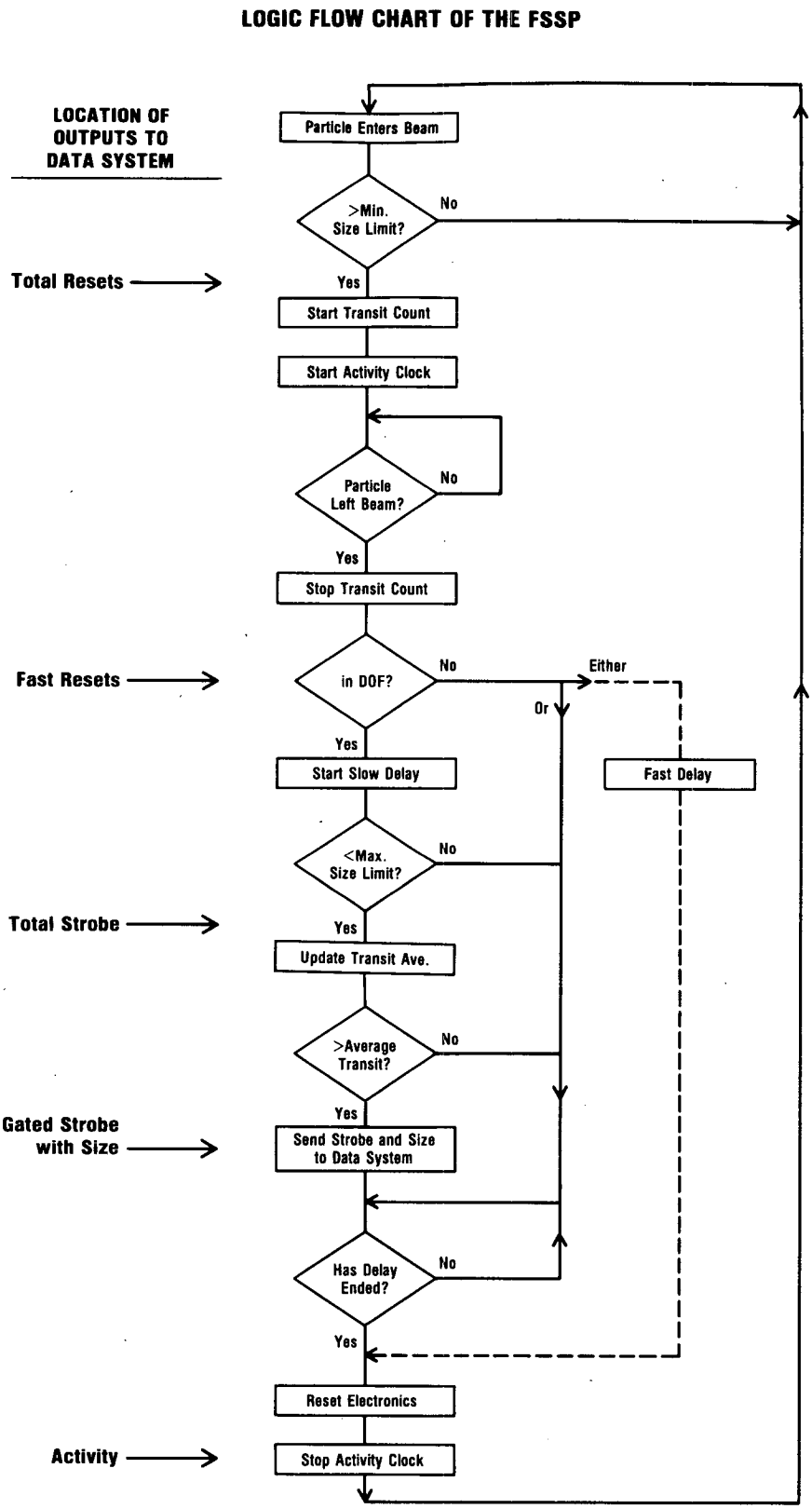

FIG. 3(a). A flowchart showing the sequence of events as a particle is detected by the FSSP. The dashed lines show the additional logic flow for probes with fast resets.

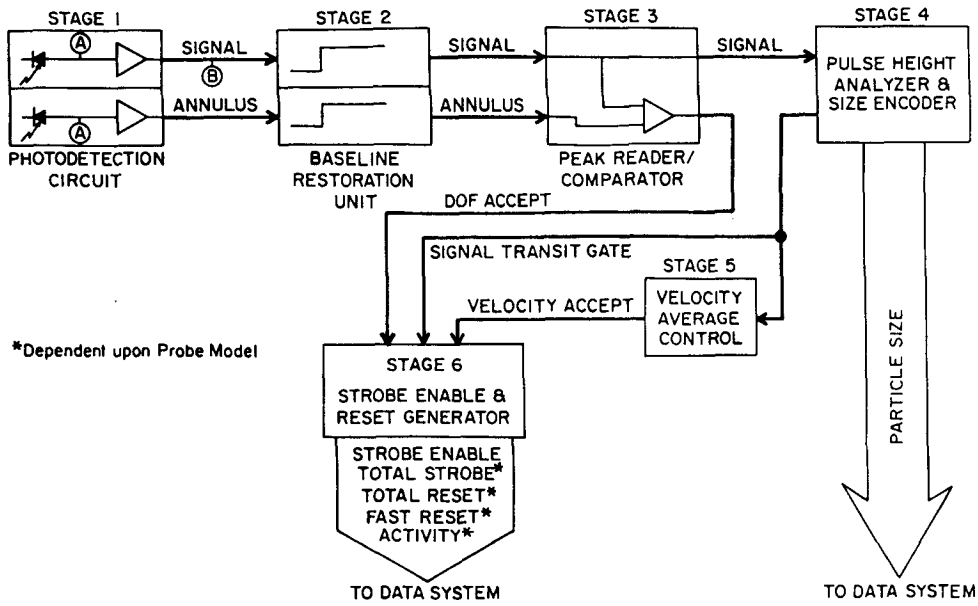

FIG. 3(b). A block diagram illustrating the basic structure and function of the FSSP electronic circuitry.

which is gated by a 10 MHz clock is compared with the average count, thus, providing the basis for velocity acceptance or rejection. If the instantaneous count is more or less than the average, the average counter is up, or down, counted in proportion (1/256) to the number of counts that the particle transit is more, or less, than the average. The new average count $\bar{C}_{i+1}$, can be given by

$$\bar{C}_{i+1} = \bar{C}_i - \frac{(C_i - \bar{C}_i)}{256}, \qquad (1)$$

where $\bar{C}_i$ is the old average and C_i is the instantaneous count. Strictly speaking, this is not a true average, as it is biased by the transit time of the most recent particles. For an airspeed of 100 m s^{-1}, a beam diameter of 0.2 mm and the clock rate of 10 MHz, a particle transit would produce about 20 counts. Thus, the resolution of transit time by the counter is relatively coarse.

The final stage provides the timing signals for the rest of the electronics, generates a pulse, which resets the electronics so that another particle can be detected, and generates various information signals, including a gated strobe pulse, to the data system when the size information is acceptable and both the DOF and velocity acceptance tests have been satisfied.

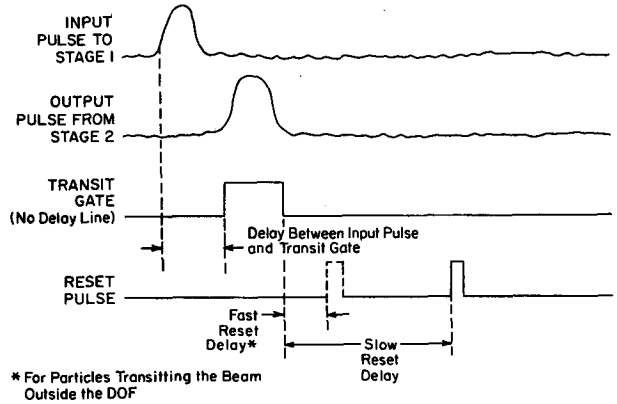

FIG. 4. A timing diagram of various voltage pulses within the FSSP electronics.

b. *Test procedures and results*

Since experimentation showed that varying the rise and fall of the input pulse made little difference in the response of the electronics, a square pulse was chosen, to simulate the waveforms produced by particles passing through the probe's beam because it is easy to measure and control.

For those tests requiring a measure of response time, the signal was injected through a 100 kΩ resistor at the output of the photodetectors (point A in Fig. 3). For those tests measuring the thresholds of the PHA size channels, the signal was injected directly into the baseline restoration unit, with the first stage disconnected (point B in Fig. 3). The results of the tests are summarized in Table 1.

The first test was to determine the delay times of each probe by injecting a pulse at point A and measuring the time from the rise of the input pulse to the rise of the reset pulse signaling the end of processing. The delay times varied from probe to

probe but agreed reasonably well with the values given by the manufacturer.

It was also discovered that there is a delay between the input pulse and transit gate (Fig. 4) as well as a minimum input pulse width (see Table 1) below which the transit gate duration would decrease no further. Particles passing through the edges of the beam with transit times shorter than the minimum will appear as if they actually passed through longer chords of the beam, thus biasing the velocity average toward longer transit times.

The PHA sizing thresholds were determined by injecting the pulse at point B and observing the size encoded by the FSSP while varying the pulse amplitude. Although different probes have different optical configurations and hence scattering angles, the PHA thresholds were quite similar from probe to probe and quite close to those specified by the manufacturer.

One set of tests was designed to observe each probe's response to the speed at which a particle passes through the beam. The input pulse was held at a fixed amplitude and frequency while varying the width and observing the voltage amplitudes at the input to the PHAs. The results of this test for two probes are shown in Figs. 5a and b for both signal and annulus responses. The 3 dB roll-off point is tabulated for all probes in Table 1. The implications of this test are twofold. First, from looking at the response of the signal voltage as the pulse width decreases, it can be seen that the signal decreases with decreasing pulse width, i.e., the measured size of a particle will decrease as the particle passes more quickly through the beam. Cerni (1983) has demonstrated this same effect with glass bead tests. Second, if the signal and annulus voltages do not decrease at the same rate with decreasing pulse width, the DOF will change. An example of this response is shown in Fig. 5b, where the annulus decreases more rapidly than the signal, thus increasing the DOF.

To observe the effect of particle arrival rate on the response of the FSSP electronics, the input pulse amplitude and width were kept constant while changing the repetition rate. The amplitude of the signal and annulus voltage were then observed at the input to the PHAs. The results of these tests for two probes are shown in Figs. 6a and b, where it may be seen that the signal and annulus amplitudes begin to decrease after a certain frequency is exceeded, a response especially evident in Fig. 6b. The implications of these results are similar to the pulse width test—particles can be undersized and the DOF can change. Figure 7 shows how the DOF changes with particle rate for the extreme case shown in Fig. 6b. Field data from this particular probe had pointed to this problem. The probe was later found to have a defective component in the baseline restoration module.

4. Optical characteristics

As with the electronic response tests discussed previously, several careful optical checks and determinations of parameters needed for accurate operation of the FSSP were made for each of the FSSPs evaluated. The optics of all probes were cleaned and aligned prior to any tests. The results of these measurements are summarized in Table 1. The beam diameters shown in Table 1 were determined by passing a 12.5 μm wire vertically through the center of the DOF using a micropositioner with 1 μm resolution. The reproducibility of this measurement was about ± 5 μm. The values shown agree well with the manufacturer's values for each probe, which are determined by projecting the beam onto a wall and visually determining the limits of the beam.

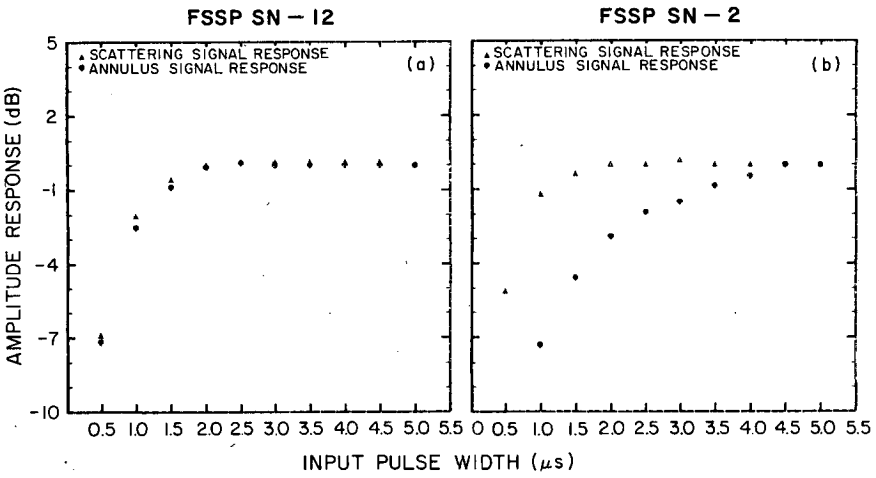

FIG. 5. Response curves of two FSSPs to different input pulse widths: (a) illustrates a typical response, whereas the response of the probe shown in (b) is abnormal and indicates malfunctioning or mismatched electronics.

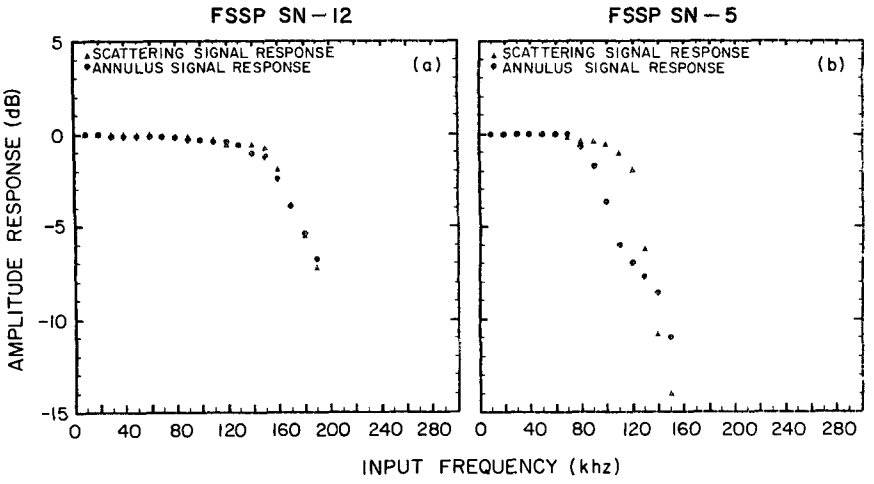

FIG. 6. As in Fig. 5 but for different frequencies.

A number of techniques were used to determine the DOF of the probes, including: 1) the diffuse tape technique used by Particle Measurement Systems (PMS); 2) a 12.5 μm metal wire or a 30 μm nylon fiber held in a support and controlled with a micropositioner and 3) droplets produced by a droplet generator. For each of these tests, the crossover points (when the signal voltage equaled the annulus voltage) were determined by moving the scattering medium back and forth along the laser beam. The diffuse tape and nylon fiber gave very similar DOFs. However, the metal wire gave a 15 to 25% larger, false DOF. The results for water droplets and also for the tape diffuser are shown in Fig. 8 for the 2–30 μm range. The diffuser technique gives results equivalent to the larger water droplets, but as the droplet size decreases below about 15 μm, the DOF begins to increase. The reason for this increase is not known. Results for the 3–45 μm range are similar but tend to give 2–4% larger DOFs than the 2–30 μm range DOF for the same droplet size. It is tempting to apply corrections for the DOF as a function of droplet diameter; however, there is appreciable uncertainty in the results for the small sizes and it is not obvious what DOF should be used for droplets less than 10 μm where the DOF is rapidly increasing. Until more measurements are available, it is probably best to use a constant DOF.

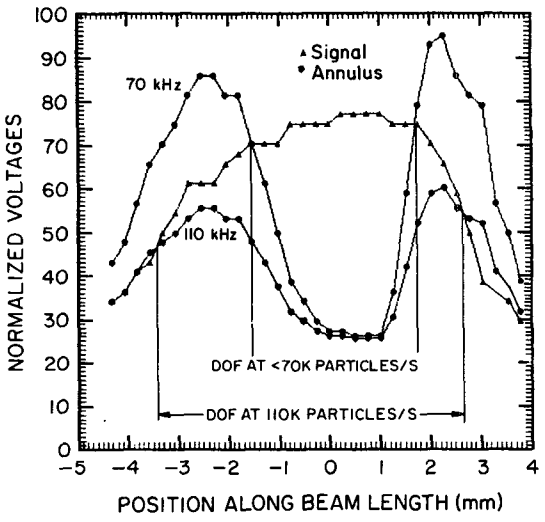

FIG. 7. The depth-of-field at two different frequencies for the FSSP frequency response curve shown in Fig. 6b.

To check the sizing of each of the probes, glass beads[3] of 3–9, 10–15, 15–25 and 25–35 μm were drawn through the probe at approximately 40 m s^{-1}. About 1000 of the beads from each of the bottles were sized with a microscope to determine the optical size distribution. Since some of the glass bead samples had long tails, the mode was chosen to represent the characteristic size of the beads rather than the mean. Also, some clumping of the beads might occur when they are drawn through the probe, thus giving an overestimate of the number of large beads. The mode was used both for the optical determination of glass bead sizes and in the processing of the FSSP data. A comparison of the optical size with that measured by the various FSSPs is shown in Fig. 9a for each instrument operating in the 2–30 μm size range. The values are corrected for the index of refraction of water based on the theoretical scattering cross sections determined by Cerni at the University of Wyoming (Cerni, 1983) for the scattering angles of acceptance shown in Table 1.

The results show slightly more scatter at sizes both larger and smaller than the 10–15 μm bead size, where PMS sets the calibration. Some of the scatter

[3] Obtained from Particle Information Services, Kingston, Washington.

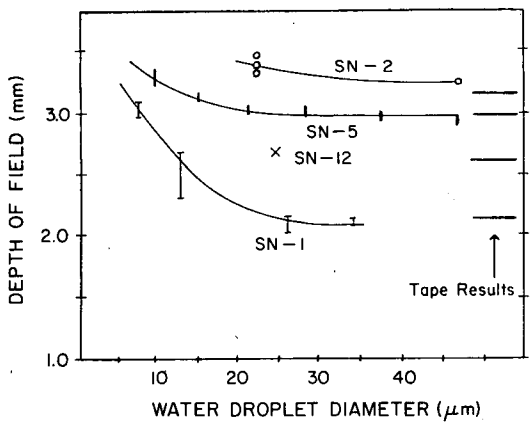

FIG. 8. Measured depth-of-field for several FSSPs as a function of water droplet diameter. Results using the manufacturer's technique with diffuse tape are shown at the right. Error bars indicate the variation in measured DOF for several separate trials.

seen in Fig. 9a is the result of experimental uncertainty. It is not uncommon to obtain differences of 1 μm from one test to another using the same set of glass beads repeatedly with the same FSSP. Most of the points shown in Fig. 9a are the average of two or more tests. This scatter shows the need for a better calibration technique. Most of the probes appear to oversize the small beads and undersize the larger ones. Part of the differences in sizing are due to differences between the PHAs and the Mie scattering curves for the various probes, a point which will be discussed further in Section 7. Figure 9b shows the results of the glass bead bests when these differences are taken into account. There is little improvement in the scatter of the results.

Laboratory studies were performed using a dropmaker (Cannon and Grotewold, 1980) to check the size calibration of FSSP number 5. Monodisperse droplets ranging from approximately 6 to 60 μm diameter were produced and drawn through the sample area of the FSSP. The size of the droplets was determined from photographs taken through a microscope using stroboscopic illumination. The results are presented in Fig. 10 and also in Fig. 9b for comparison with the glass bead tests. Considering the error in the measurement of about ±1 μm, the sizes measured by the FSSP agree reasonably well with the actual droplet diameters, although there is a suggestion of oversizing of droplets < 14 μm in diameter in the 2–30 μm operating range. This is consistent with the glass bead results of Fig. 9. The uncertainty in these measurements does not permit a definitive statement of measurement accuracy, but serves to show the general validity of the scattering technique. Similar calibrations done a few years ago showed different calibrations for different probes, comparable to the results obtained from the glass bead tests presented herein.

This same setup was used to determine the artificial spreading of the spectrum caused by droplets transitting the beam in different positions. The results are shown in Fig. 11 for drops sized photographically at 26 μm. For a velocity acceptance ratio of 0.5, approximately 5% were sized at 28 μm, 65% at 26 μm and 30% at 24 μm. This broadening also can be observed from glass bead calibrations as shown in Fig. 12 and previously demonstrated by Cerni (1983). Spray comparison results presented below show that broadening of the spectrum varies from probe to

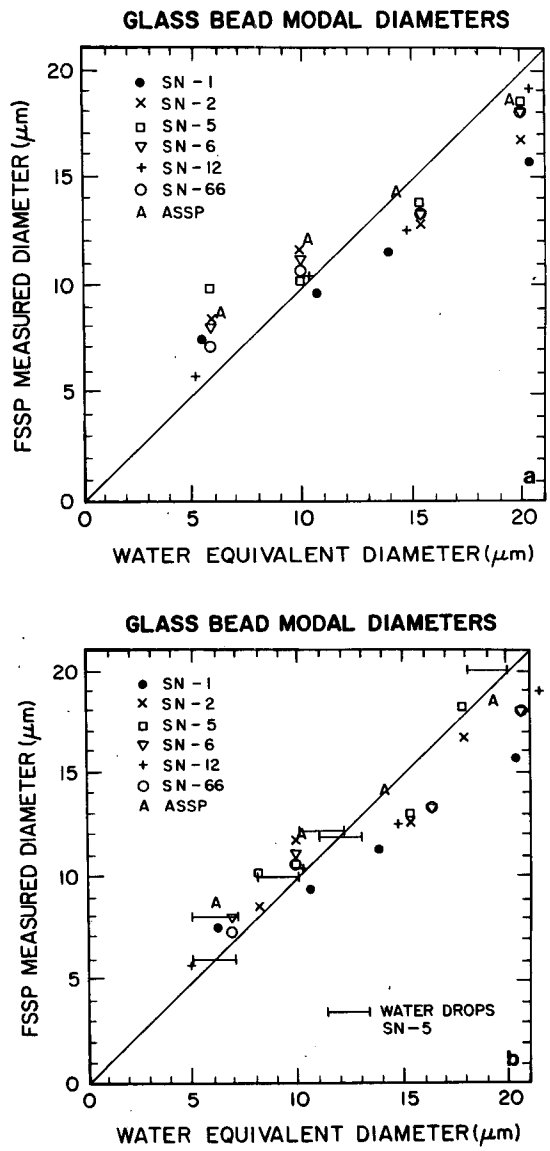

FIG. 9. The *modal* diameter of glass bead samples measured by several FSSPs operating in the 2–30 μm range plotted as a function of the water equivalent of the *modal* diameter: (a) No correction for the difference between the PHA and the theoretical Mie scattering curve; (b) Correction made for this difference. The corresponding water droplet tests of Fig. 10 are shown with error bars.

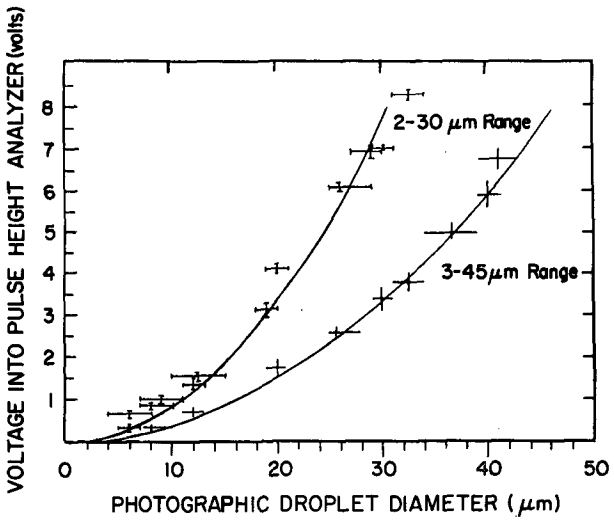

FIG. 10. Comparison of water droplet sizes measured by FSSP serial number 5 with sizes determined from photomicrographs of the droplets. The ordinate shows the peak pulse voltage levels measured immediately before the PHA. The vertical and horizontal error bars reflect the variation in peak pulse amplitude and uncertainty in size determination from the photographs, respectively. The solid lines are the expected relation between voltage and droplet size as specified by the manufacturer's calibration.

probe and is probably dependent upon the optical configuration, location and number of modes in the laser beam, the velocity acceptance ratio and the electronic response of each probe. The results of Fig. 11 are applicable for this FSSP alone.

5. Comparisons using a spray device

Prior to the CCOPE field season, a device that produces a droplet spray that can be blown past various sensors was developed as a ground test unit (Dye, 1983). A modified version of this device was used to compare the FSSPs at the December workshop. For these tests, a distance from the spray nozzle of about 60 cm and airspeeds of 60, 80 and 100 m s^{-1} were used. Six different settings of the water flow

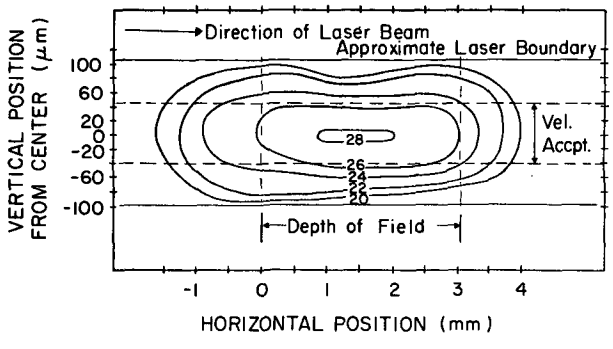

FIG. 11. Droplet diameters measured by an FSSP in different parts of the DOF for uniformly sized 26 μm diameter drops.

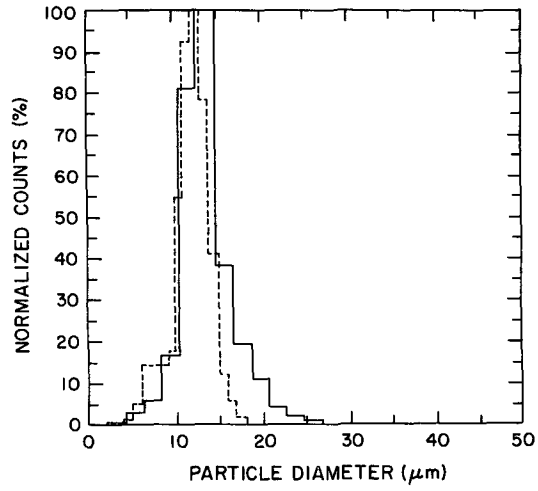

FIG. 12. A comparison of glass beads sized from microphotographs (dashed) and by an FSSP (solid).

rate produced droplet concentrations ranging from approximately 100 to 1200 droplets cm^{-3} and mean diameters from about 6 to 12 μm. All results presented below are 30 s averages from those tests, for which the spray device was operating continuously at constant airspeed and water setting and switched directly from one FSSP to another. This minimized differences due to evaporation and variations in the spray pattern. All data were digitally recorded on tape by the NCAR/Research Aviation Facility (RAF) aircraft recording system (ARIS IV) and were processed with the same software on the RAF ground-based computer system. Housekeeping information on total strobes, total resets, activity and fast resets (if applicable) were recorded for each probe. An example of the spectrum measured by two of the FSSPs in the midrange of the water flow settings is shown in Fig. 13.

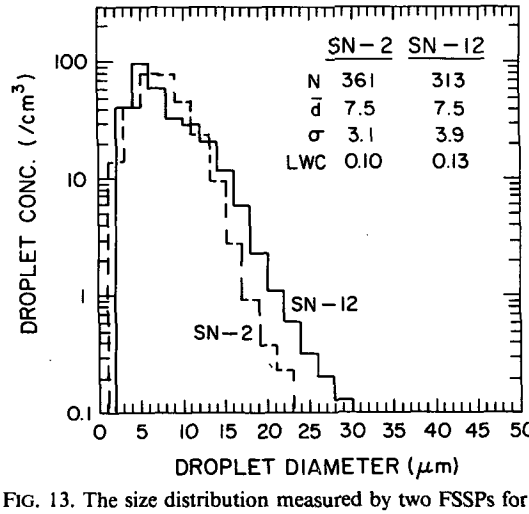

FIG. 13. The size distribution measured by two FSSPs for the same spray of droplets moving through the FSSPs at 80 m s^{-1}.

Two series of figures for two separate pairs of FSSPs are shown in Figs. 14a–d and Figs. 15a–d to illustrate some of the trends seen in the comparisons. Although the uncorrected concentrations (Figs. 14a and 15a) show good agreement at low concentrations, the disagreement increases to as much as 30% (Fig. 15a) for the highest concentration. When a modified dead time correction of the form proposed by Baumgardner (1983) and discussed later is made to the concentration measurements, differences are normally less than 15%. Given the uncertainties (Baumgardner, 1983) in the determination of the DOF (±5%), beam diameter (±5%), airspeed of the flow through the sample area (±5%) and activity correction factor (accuracy unknown), it is not surprising to find differences of 15% among the probes.

Sizing differences between the various instruments are illustrated in Figs. 14b and 15b for mean diameter and in Figs. 14c and 15c for standard deviation or spread of the spectrum. Figure 13 shows the comparative distributions, after the dead time correction, for

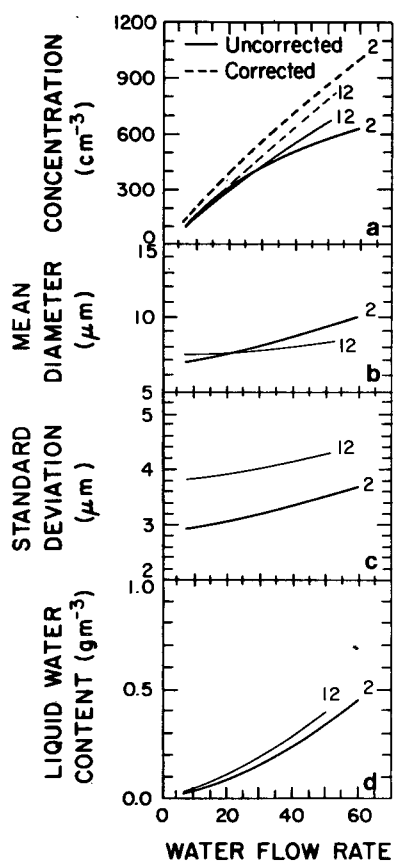

FIG. 14. Parameters measured by FSSPs serial numbers 2 and 12 operating in the 2–30 μm range plotted as a function of water flow rate in the spray device operating at 80 m s^{-1}. (a) uncorrected (solid) and corrected (dashed) concentration, (b) mean diameter, (c) standard deviations about the mean diameter and (d) derived liquid water content (corrected).

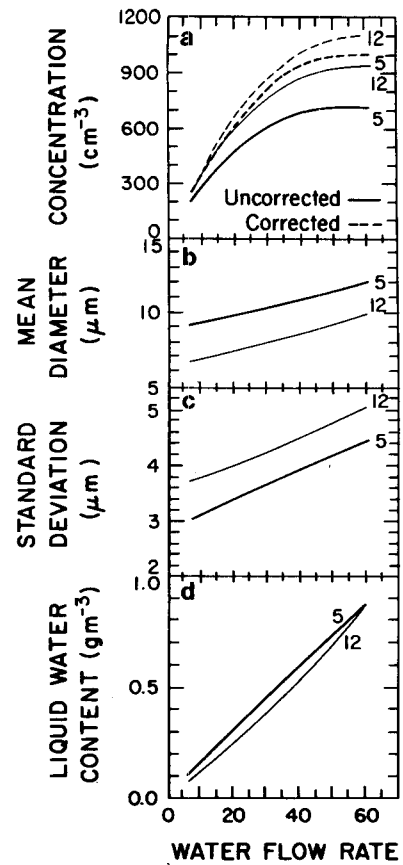

FIG. 15. As in Fig. 14 except for FSSPs 12 and 5 with the spray device operating at 60 m s^{-1}.

the same pair of instruments compared in Fig. 14. As seen in these figures, shapes of the distributions as characterized by the mean diameters and the standard deviations were often quite different. The differences in distribution measured by the individual probes were, in part, a result of the optical and electronic configuration of each probe. For example, probes 2 and 5 in Figs. 14 and 15 have the same optical configuration and only one set of comparators in the PHA. Probe 12 has separate comparators for each range and a different scattering angle. The figures show that these two probes gave smaller standard deviations and larger mean diameters than probe 12. Probe 12 consistently yielded the largest standard deviation or spread of the spectrum. The one ASSP tested also had a large minimum scattering angle and yielded broad distributions. Relationships of this nature need further investigation.

The two pairs of probes shown in Figs. 14 and 15 measured nearly the same liquid water content even though the mean diameters were quite different. This was not true for all the probes tested. Some differed by as much as 100% at some flow settings. In these figures the difference in mean diameter appears to be offset by the difference in the standard deviation and

concentration. The liquid water contents presented in these figures were calculated using the modified dead time correction for concentration, and the data from all probes were processed using the same software and the same channel widths in a particular range.

6. Sizing corrections

The sizing resolution and accuracy of the FSSP is limited by inhomogeneities in the laser beam, ambiguities in the Mie scattering curves and by the accuracy to which the probe can be calibrated. The sizing is also a function of airspeed as a result of the response time of the probe electronics. The most commonly used calibration technique and that recommended by PMS is to draw glass beads, particularly those 10–15 μm in diameter, through the sample area at a speed appropriate for the intended use. The measured spectrum then needs to be corrected for the difference between the index of refraction of glass and that of water to obtain the water equivalent diameter, as illustrated in Fig. 16. While this provides a useful check of the gain of the system, there is some uncertainty inherent in this check. First of all, in the 10 to 15 μm region, multiple peaks in the Mie curve can lead to 2 or even 3 water equivalent diameters (Fig. 16). Because there is less relative variation in the Mie curves at larger sizes, it is better to calibrate at several bead sizes and to give more weight to the larger beads: 25–35 μm for the 2 to 30 μm range and 35–45 μm for the 3 to 45 μm range. For aerosol measurements in the 1 to 15 μm range, where sizes less than 10 μm are of primary interest and the Mie peaks are pronounced, Pinnick *et al.* (1981) suggest redefining channel limits and combining channels to remove the ambiguity in sizing.

Even after the gain has been set correctly and the optics have been aligned properly, systematic errors in sizing can occur because of differences between the Mie curve for that instrument and the PHA threshold settings. For some probes tested, the differences were minimal while for others the error was appreciable. The PHA threshold curve for the 2–30 μm range is compared in Fig. 17 with the theoretical Mie scattering curve for each configuration of the FSSP used in this study–three sets of scattering angles and single and multiple PHA models. Similar figures can be constructed for the other ranges. In each of the plots the PHA curve has been adjusted vertically to fit the Mie curve best at 10 to 11 μm diameter, the modal water equivalent diameter of the 10–15 μm glass beads. The fit of the PHA curve to the Mie

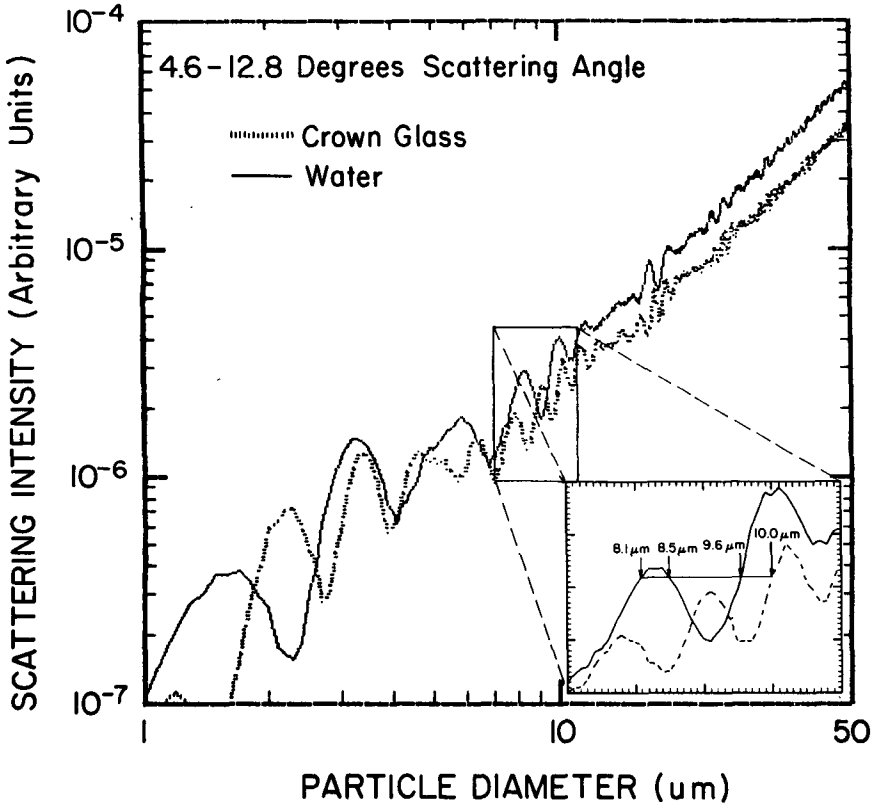

FIG. 16. A plot of the Mie function showing the intensity of scattered light as a function of particle diameter for crown glass and water particles. The inset shows an expanded view of a section of these curves in a linear plot.

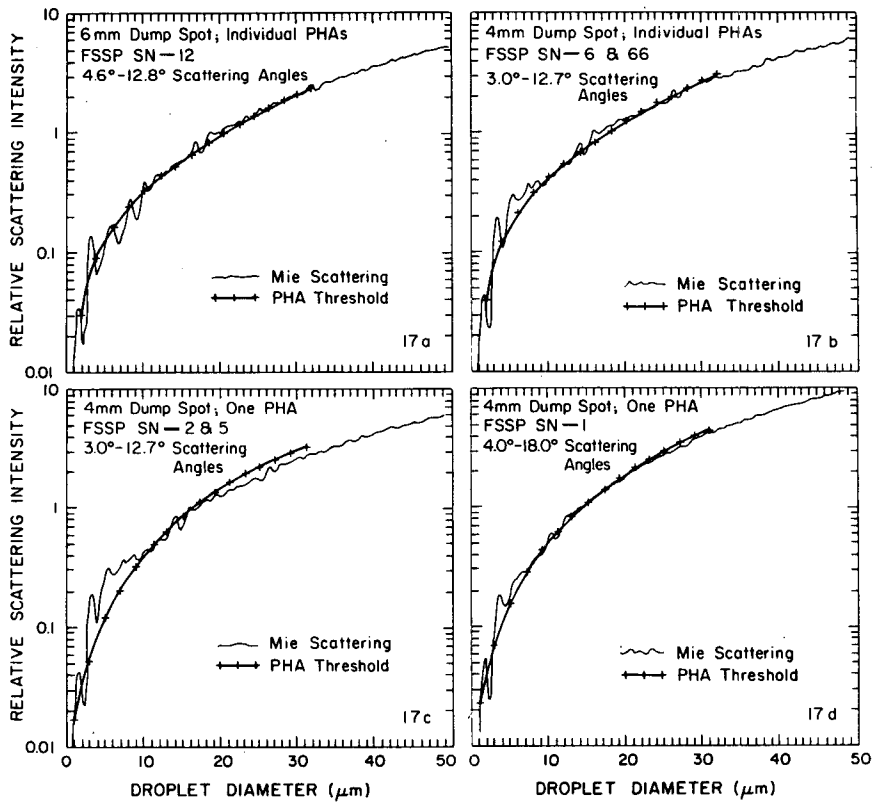

FIG. 17. A comparison of the theoretical Mie scattering curve with the PHA threshold curve for FSSPs with four different optical-electronic configurations. FSSP SN 1 with the original FSSP optical configuration has a 50 mm collecting lens. The others have 55 mm collecting lenses.

curve is reasonable for Figs. 17a and d, marginal for Fig. 17b, but shows appreciable oversizing of droplets < 10 μm and undersizing of droplets > 20 μm for Fig. 17c.

One of the probes (number 5) with the configuration represented by Fig. 17c is flown on the NCAR/NOAA sailplane. Corrections were made to the channel size definitions for this probe by using a smoothed Mie curve and determining the diameters most closely corresponding to the PHA comparator settings. Table 2 shows these new channel definitions along with the standard ones. A comparison of measured liquid water content using the two different channel definitions is shown in Fig. 18 for a case in which the sailplane ascended from cloud base to 3000 m above base in a growing continental cumulus cloud. Independent measurements showed the lower part of this ascent to be in an adiabatic region of the cloud, hence, the adiabatic value of the liquid water content (LWC) is shown for comparison. Mean droplet diameter increased from 6 μm diameter near cloud base (1620) to 15 μm at 1300 m above base (1625). The correction to the channel definitions improved the agreement between the measured value of the LWC and the adiabatic value, however, the measured values still seem to be high for the first couple of minutes, suggesting that the correction was not quite large enough in the small droplet region.

As discussed in Section 3, the amplitude response of the FSSP signal-conditioning electronics causes

TABLE 2. FSSP channel definitions for the sailplane 2–30 μm nominal range.

Channel	Standard limits	Modified limits	Midpoint	Width
1	1–3	1.0–2.3	1.65	1.3
2	3–5	2.3–3.2	2.75	0.9
3	5–7	3.2–4.9	4.05	1.7
4	7–9	4.9–7.4	6.15	2.5
5	9–11	7.4–11.0	9.2	3.6
6	11–13	11.0–13.0	12.0	2.0
7	13–15	13.0–14.8	13.9	1.8
8	15–17	14.8–16.6	15.7	1.8
9	17–19	16.6–19.2	17.9	2.6
10	19–21	19.2–22.6	20.9	3.4
11	21–23	22.6–25.2	23.9	2.6
12	23–25	25.2–27.0	26.1	1.8
13	25–27	27.0–30.0	28.5	3.0
14	27–29	30.0–33.0	31.5	3.0
15	29–31	33.0–35.2	34.1	2.2

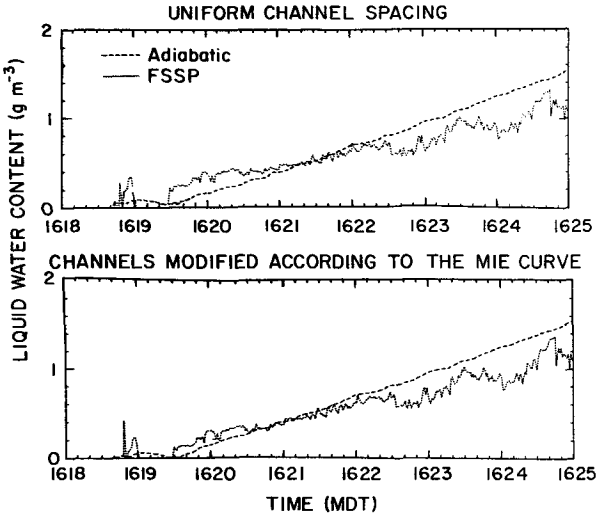

FIG. 18. A comparison between liquid water content calculated from the droplet spectra measured by the FSSP used on the NCAR/NOAA sailplane, for the cases of uniform channel spacing and channel thresholds suggested by the Mie scattering curve for that instrument. The dashed line shows the adiabatic value calculated for unmixed parcel ascent based on measured cloud base parameters.

particles to be undersized as the optimum range of particle rates and airspeeds is exceeded. This behavior was seen when particles enter the beam at rates higher than $\sim 10^5$ s^{-1} (about 400 droplets cm^{-3} for an airspeed of 100 m s^{-1}), or when the particle's transit time is faster than 1.0–1.5 μs (100–130 m^{-1} depending on effective beam diameter). In most cases the individual FSSPs have been manufactured to suit the needs of individual users, particularly in terms of airspeed. Figure 19 shows an example of how the size determination by the FSSP changes with increasing airspeed. These results were derived from measurements of the pulse width response of probe 6 shown in Fig. 5a. The pulse width is converted to an airspeed using the average width of the laser beam divided by the pulse width. The limiting values differ from probe to probe, but the aforementioned values are near the upper limit of proper operation for any of the probes tested.

Cerni (1983) also has studied the effect of airspeed on sizing in laboratory experiments in which glass beads were accelerated past the sampling area at different airspeeds. He used the counts from the velocity averaging circuitry to determine the speed of beads passing through the sample area. However, for data processing, airspeeds measured elsewhere on the aircraft are used. This uncertainty in airspeed introduces some uncertainty (probably less than 10%) in our results and those of Cerni (1983). Flow distortions due to mounting locations can also influence the measurements. Checks of the airspeed from the averaging circuit with independent airspeed measurements both in free air and through the FSSP sampling tube are needed to reduce the uncertainty for sizing corrections and also for the calculation of the concentration discussed in the following section.

7. Concentration corrections

The accuracy of measuring the particle concentration depends upon an accurate measurement of the FSSP sampling volume, as well as on the detection of all particles within that volume. The sampling volume is determined by the DOF, the beam diameter, the airspeed and the sampling period. Under static conditions, the DOF may be measured within 5% by simultaneously measuring the annulus and signal voltages as a thin, translucent scattering medium is moving along the laser beam (Fig. 2). Dynamically, the DOF can change if the frequency response of the signal and annulus electronics are not well-matched as in the case shown in Fig. 6b. Similarly, DOF changes can occur when pulse widths become less than 1.0 μs. This condition of unmatched frequency response of the signal and annulus electronics at rates less than 10^5 s^{-1} and airspeeds less than 100 m s^{-1} is a malfunction of the probe and should be rectified. However, if such a condition exists during instrument use, it is possible to make some corrections. Using electronic tests to establish the frequency response and then plotting figures of the type of Figs. 5 and 6, a relationship between DOF and particle rate or pulse width may be derived, as demonstrated by Fig. 7.

The velocity averaging circuit was designed to reject particles that pass through the outer portion of the beam in order to define an *effective beam diameter* in which sizing would be more accurate. Measurement of the total strobe output allows the effective diameter

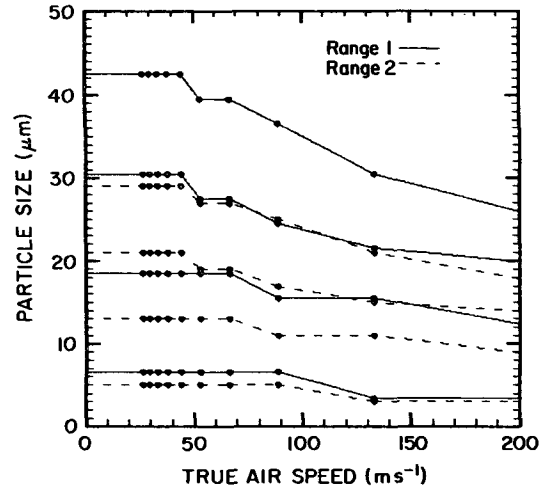

FIG. 19. The particle sizes that an FSSP would measure as a function of airspeed for particles of 7.5, 18.5, 30.5 and 42.5 μm within the 1 to 47 μm range, and 5, 13, 21, 29 within the 1 to 31 μm range. The discontinuities are a result of the width of the channels in which the particles would be sized.

in the vertical to be determined since the ratio of gated to total strobes, the *velocity acceptance ratio,* is just the fraction of the vertical beam diameter within which particles are velocity accepted. Theoretically, this effective beam diameter is about 62% of the total diameter; however, empirical tests show that typical values vary from 40 to 70% from probe to probe. Figure 20 is an example of this fraction as a function of total strobes. From this plot it is obvious that even though the mean for this probe is approximately 50%, there are large deviations from this mean which reflect real changes in sample volume used by the probe in accepting particles for counting and sizing. If a fixed effective beam diameter (velocity acceptance ratio) is used, these variations can introduce large sample volume errors (as much as 20–30%) if only a fixed effective beam diameter is used. It is disconcerting that the velocity acceptance ratio is so variable for a given probe and that different probes display typical values that are so widely different and so far from the theoretical value. Part of this difference and scatter may be due to the coarse resolution of the transit time average (see Section 3), but one must also wonder about the symmetry of the beam and the functioning of the logic circuitry that decides which particles will be accepted in the DOF and have greater than average transit velocity. Also, the current methods of determining total beam diameter do not give us the diameter of the beam over which particles actually are detected, but rather give the visual diameter. These considerations suggest that the error in the effective beam diameter could be larger than 5%.

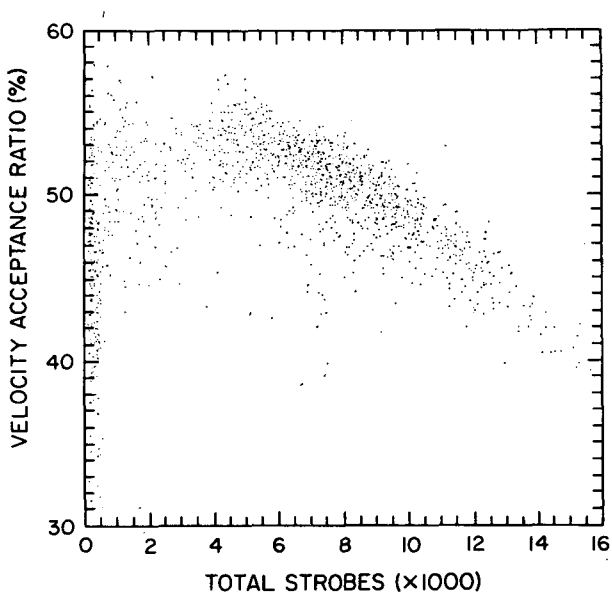

FIG. 20. In-cloud data on the velocity acceptance ratio plotted as a function of total strobes for an FSSP operated on an aircraft flying at 80 m s^{-1} in stratus clouds.

When the velocity acceptance ratio (VAR) is utilized to compensate for changes in the effective beam diameter, the measured concentration N_m in each channel is given by

$$N_m = \frac{n_m}{(\mathrm{BD})(\mathrm{VAR})(\mathrm{DOF})(\mathrm{TAS})\Delta t}, \qquad (2)$$

where n_m is the number of counts in that channel per unit time, BD total beam diameter, TAS the true airspeed and Δt the sampling period.

As a result of particles passing through the sample volume during the electronic dead time or being coincident in the beam, the concentration measurements will be underestimated. For most probes these losses begin to be important when concentrations exceed a few hundred per cubic centimeter. A good estimate of these losses can be made if the fraction of the sampling period when the FSSP was actively processing particles is known. This activity period must include both the time that particles were transitting the beam and the time that the electronics were processing data and being reset. The activity output discussed previously provides such an estimate. As discussed by Baumgardner (1983) the correction equation takes the form

$$N_a = \frac{N_m}{1 - mA}, \qquad (3)$$

where N_A is the actual concentration and m is a probe-dependent correction factor to the activity A. The correction factors m for the probes in this study were determined using a computer model to simulate the response of the FSSP probes (Baumgardner, 1982) and are tabulated in Table 1. Cerni (1983) corrected his data using the same equation as (3). However, he derived the factor m using laboratory simulations. The value he derived of 0.54 agrees well with the value used in these studies of 0.56 (SN 12, Table 1). Without an activity correction of this type, errors in measured concentrations can exceed 100% when the actual concentration approaches 1000 cm^{-3}. A formulation that incorporates individual and more exact corrections for coincidence errors and dead time losses is being worked out and will be reported in a future paper.

8. Diagnostic aids

One method of monitoring the performance of the FSSP to detect possible malfunctions is to look at the *DOF fraction* as a function of total resets, where the DOF fraction is the ratio of total strobes to total resets. This ratio is approximately the same as the ratio of DOF to total sensitive beam length. This ratio should remain nearly constant as the particle rate (represented by total resets) increases. As Fig. 21 illustrates, the electronic response seen in Fig. 6b

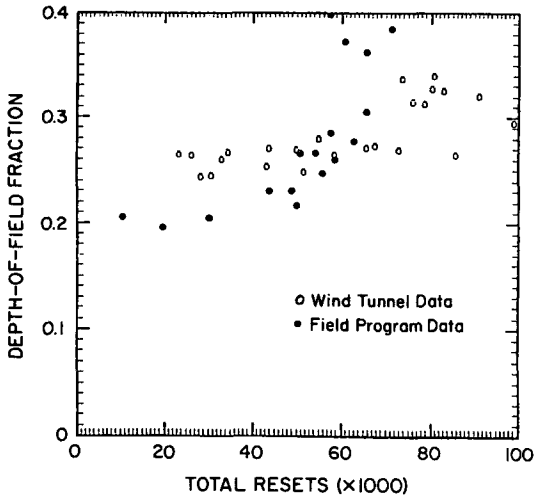

FIG. 21. An illustration of the depth-of-field fraction as a function of the total resets demonstrating the frequency response problem of the probe whose response was shown in Fig. 6b.

shows a marked increase of the DOF fraction with increasing total resets in both aircraft and wind tunnel measurements. The difference in response between the wind tunnel and flight data is a reflection of the nonuniform pattern of the spray in the wind tunnel. In a similar manner, monitoring of the velocity acceptance ratio, the ratio of the number of particles velocity accepted to the total strobes, can aid in identifying other malfunctions in the electronic circuitry.

9. Concluding remarks

Since its initial development, modifications have been made to improve the performance of the FSSP. Thus, the limitations of and the accuracy that can be achieved with an FSSP is, to some degree, dependent upon the features that are incorporated in that particular probe. These limitations are primarily a result of electronic response, optical resolution and calibration uncertainties.

The features that differ from probe to probe and, hence, should be known for each probe are as follows:

- The scattering angles over which light is collected.
- The focal length of the collecting lens.
- The diameter of the laser dump spot.
- The various delay and reset times.
- Does the probe have fast resets and are total strobes, total resets and activity recorded?
- Are there individual sets of comparators for each size range in the PHA or only one set?
- The frequency and pulse width response of signal and annulus electronics.

While some of the limitations and features are specific to a particular probe, there are some general requirements that must be considered if one wants to optimize the size and concentration measurement accuracy. Some of these may seem obvious, but in the process of conducting these studies and in checking other FSSPs, we have run across more than one probe that was not clean or aligned properly, or for which incorrect DOF or beam diameters were being used. The checks which are considered important are:

1) The DOF and beam diameter measurements provided by the manufacturer are valid; however, they need to be checked after transport and occasionally in the field during use.

2) Routine checks must be made to be certain the optics are clean and aligned properly. Glass bead calibrations can help detect problems, but direct inspection is also necessary.

3) Because of the tail in some glass bead samples and the possibility of bead clustering, it is better to use the modal diameter of the measured spectrum rather than the mean diameter when calibrating the instrument. Several sizes of glass beads should be used to establish the calibration curve. The larger beads, particularly the 25–35 μm beads for the 2–30 μm sizing range of the FSSP, are more sensitive than smaller beads for establishing the proper gain.

4) Because of the complex optical–electronic interaction in the FSSP, the optical characteristics and electronic response should be known for each instrument. In particular, the frequency and pulse width response of the signal and annulus must be well matched if concentrations greater than approximately 500 cm^{-3} are to be measured or if the probe is flown on an aircraft flying at speeds of 100 m s^{-1} or more.

5) A dead time and coincidence correction is needed for most airborne measurements when particle concentrations exceed a few hundred per cubic centimeter. These corrections require additional housekeeping information on total strobes, total resets or activity and, if applicable, fast resets.

6) If accurate sizing is desired, some corrections may be necessary to compensate for the difference between the theoretical Mie scattering curve for the pertinent acceptance angles and the comparator levels of the PHA curve. This is particularly important for FSSPs with only one PHA.

7) As shown by the electronic response tests and by Cerni (1983), if the instrument is to be flown at speeds > 100 m s^{-1}, corrections need to be made to the measured sizes to correct for undersizing.

8) The FSSP does cause artificial broadening of the droplet spectrum. The broadening varies from probe to probe and is difficult to quantify and to correct.

Acknowledgments. We would like to thank the participants in the FSSP workshop for their help and discussion. They include J. Walter Strapp of the

Atmospheric Environment Service of Canada, Todd A. Cerni of the University of Wyoming and Lawrence F. Radke of the University of Washington. We also would like to thank Walter Grotewold for fabrication of test devices and his assistance with the droplet studies, Todd A. Cerni for providing the appropriate Mie scattering curves, and J. Walter Strapp and Warren King for comments on this paper and valuable discussion of various aspects of the FSSP.

REFERENCES

Baumgardner, D., 1982: A computer simulation of the forward scattering spectrometer probe. *Preprints Conf. on Cloud Physics,* Chicago, Amer. Meteor. Soc., 279–281.

——, 1983: An analysis and comparison of five water droplet measuring instruments. *J. Climate Appl. Meteor.,* **22,** 891–910.

Breed, D., and J. Dye, 1982: In-cloud intercomparisons of FSSP and JW probes during CCOPE. *Preprints Conf. on Cloud Physics,* Chicago, Amer. Meteor. Soc., 282–285.

Cannon, T., and W. Grotewold, 1980: Improved drop generators for calibration of drop spectrometers and use in laboratory cloud physics experiments. *J. Appl. Meteor.,* **19,** 901–905.

Cerni, T. A., 1983: Determination of the size and concentration of cloud drops with an FSSP. *J. Climate Appl. Meteor.,* **22,** 1346–1355.

Dye, J. E., 1983: A spray device for ground testing of the Johnson-Williams liquid water content meter. *Preprints Fifth Symp. on Meteorological Observations and Instrumentation,* Toronto, Amer. Meteor. Soc. and Can. Meteor. and Ocean. Soc., 362–365.

Gayet, J. F., 1976: Sur les performances de L'ASSP-100 de Knollenberg pour la granulometrie des nuages. *J. Rech. Atmos.,* **10,** 105–118.

Knollenberg, R. G., 1976: Three new instruments for cloud physics measurements. *Preprints Int. Conf. on Cloud Physics,* Boulder, Amer. Meteor. Soc., p. 554.

——, 1981: Techniques for probing cloud microstructure. *Clouds: Their Formation, Optical Properties and Effects,* P. V. Hobbs and A. Depak, Eds., Academic Press, 15–19.

Mossop, S. C., 1983: Intercomparison of instruments used for measurement of cloud drop concentration and size distribution. *J. Climate Appl. Meteor.,* **22,** 419–428.

Pinnick, R. G., D. M. Garvey and L. D. Duncan, 1981: Calibration of Knollenberg FSSP light-scattering counters for measurement of cloud droplets. *J. Appl. Meteor.,* **20,** 1049–1057.